GPS Solutions (2019) 23:81
https://doi.org/10.1007/s10291-019-0873-8

ORIGINAL ARTICLE

Multi-GNSS inter-system biases: estimability analysis and impact on RTK positioning

Xiaolong Mi[1,2] · Baocheng Zhang[1] · Yunbin Yuan[1]

Received: 4 January 2019 / Accepted: 31 May 2019 / Published online: 5 June 2019

Abstract
Inter-system biases (ISB) are of great relevance for the combined processing of the code and phase data of multiple global navigation satellite systems (GNSSs). Calibrating the ISB makes it possible to enhance the interoperability among different GNSS constellations and thus benefits multi-GNSS-based positioning, navigation and timing applications. Initial investigations of the characteristics of ISB have been carried out, usually making use of overlapping frequencies and adopting the double-differenced (DD) model. However, this approach seems inapplicable when dealing with ISB for non-overlapping frequencies. We identify the estimability of the ISB by using the ionospheric-float, ionospheric-fixed and ionospheric-weighted models formulated on the basis of between-receiver single-differenced (SD) multi-GNSS observation equations, resulting in the so-called SD method, which is capable of estimating the ISB in case of both overlapping and non-overlapping frequencies. Using dual-frequency data for short and medium baselines, we analyze 30-s epoch-by-epoch estimates of the GPS–Galileo and GPS–BDS ISB. The quantitative results indicate that the same conclusion is reached using either the SD method or the customary method based on DD observations (called the DD method); that is, the code and phase ISB time series are both approximately constant on a time scale of a few days from a statistical perspective. However, the SD method has the advantage that it can be used to flexibly estimate ISB for both overlapping and non-overlapping frequencies and thus can be better applied for real-time kinematic positioning than the DD method. Furthermore, the multi-GNSS positioning accuracy using inter-system differencing can be improved by 20–35%, as compared to the SD classical differencing in which *S*-basis is selected per constellation, thanks to the reasonable calibration of the ISB.

Keywords Global navigation satellite systems (GNSSs) · Inter-system biases (ISB) · Ionospheric-fixed model · Ionospheric-weighted model · Ionospheric-float model · Real-time kinematic (RTK)

Introduction

The emergence of multiple satellite navigation systems, including BDS, Galileo, modernized GPS and GLONASS, is presenting great opportunities and challenges for both scientific and engineering applications (Li et al. 2015). This situation offers the potential to enlarge the field of global navigation satellite systems (GNSSs) applications while simultaneously improving the existing positioning, navigation and timing (PNT) services (Liu et al. 2018; Zhang et al. 2018). The main benefit of taking advantage of a multi-GNSS and multi-frequency data is the ability to achieve better accuracy, integrity and availability than is possible using data from only one GNSS (Li et al. 2017; Wang et al. 2016b).

However, inter-system biases (ISB) must be considered when performing the combined processing of data from different GNSSs (Dalla Torre and Caporali 2015; Paziewski et al. 2015). By definition, the ISB are actually the offsets between the hardware delays experienced by multi-constellation signals inside a receiver, which depend on the correlations inside the receiver and may reach up to hundreds of nanoseconds (Nadarajah et al. 2013; Odijk and Teunissen 2012; Paziewski and Wielgosz 2014). Moreover, ISB exist not only for the code signals but also for the phase signals (Jiang et al. 2017; Nadarajah et al. 2014).

✉ Baocheng Zhang
b.zhang@whigg.ac.cn

[1] State Key Laboratory of Geodesy and Earth's Dynamics, Institute of Geodesy and Geophysics, Wuhan, China

[2] University of Chinese Academy of Sciences, Beijing, China

At present, most studies of ISB have focused on overlapping frequencies, whereas recent studies have addressed non-overlapping frequencies or the mixed processing of non-overlapping and overlapping frequencies (Gioia and Borio 2016; Tian et al. 2017). Moreover, the double-differenced (DD) model on which ISB estimation is typically based cannot be easily extended to the case of non-overlapping frequencies (Gao et al. 2017; Odijk et al. 2016). Considering that the number of frequencies shared by any two GNSS constellations is small, it is imperative to develop an ISB estimation method that is suitable for both overlapping and non-overlapping frequencies.

In this contribution, we propose a method of ISB estimation based on between-receiver single-differenced (SD) GNSS observations, which is applicable for the estimation of ISB for non-overlapping frequencies. We formulate the estimability of the ISB for the ionospheric-float, ionospheric-fixed and ionospheric-weighted models by applying *S*-system theory to resolve the rank deficiencies underlying multi-frequency dual-GNSS relative positioning models with and without ionospheric constraints. We then use the proposed SD method to characterize the ISB between GPS, BDS and Galileo for different types of receivers separated by several short and medium baselines. Regarding the BDS constellation, we consider the impact of different satellite types, namely satellites in medium-altitude earth orbit (MEO), geostationary orbit (GEO) and inclined geosynchronous (IGSO) on the ISB estimation. Furthermore, the benefits for short-, medium- and long-baseline real-time kinematic (RTK) positioning that are provided by the calibration of the ISB are analyzed.

The next section briefly describes three multi-GNSS functional models that are formulated on the basis of between-receiver SD observables and can be used for estimating the ISB: the ionospheric-float, ionospheric-fixed and ionospheric-weighted models. In the subsequent section, the results of ISB analyses based on several sets of data are presented for the GPS–Galileo and GPS–BDS cases. That section also describes the RTK performance for short, medium and long baselines, for which the ISB are treated as time-invariant unknowns because of their stability.

Methods

This section discusses the ionospheric-float, ionospheric-fixed and ionospheric-weighted models. After addressing the rank deficiencies underlying these models, we focus on the estimability of the ISB, which applies to both overlapping and non-overlapping frequencies.

Estimation of ISB using the ionospheric-float model

The SD code and phase observation equations for two different GNSS constellations are linearized as follows:

$$\begin{aligned} E\left\{p_j^{s_A}\right\} &= g^{s_A}x_r + \mathrm{d}t + d_j^A + \mu_j^A I^{s_A} \\ E\left\{\phi_j^{s_A}\right\} &= g^{s_A}x_r + \mathrm{d}t + \delta_j^A + \lambda_j^A N_j^{s_A} - \mu_j^A I^{s_A} \\ E\left\{p_l^{q_B}\right\} &= g^{q_B}x_r + \mathrm{d}t + d_l^B + \mu_l^B I^{q_B} \\ E\left\{\phi_l^{q_B}\right\} &= g^{q_B}x_r + \mathrm{d}t + \delta_l^B + \lambda_l^B N_l^{q_B} - \mu_l^B I^{q_B} \end{aligned} \tag{1}$$

Here, the symbol s_A (or q_B) represents a satellite, and the symbol j (or l) represents a frequency. A and B denote the two different GNSS constellations. $p_j^{s_A}$ and $p_j^{q_B}$ refer to the SD code observables, while $\phi_j^{s_A}$ and $\phi_l^{q_B}$ refer to the SD phase observables, for which the approximate geometric range and the hydrostatic component of the tropospheric delay are corrected a priori. g^{s_A} or g^{q_B} is the receiver-to-satellite unit vector, and x_r denotes the receiver coordinates. The receiver-dependent unknowns are represented as follows: The receiver clock error is $\mathrm{d}t$, the receiver code bias is d_j^A (or d_l^B), and the receiver phase bias is δ_j^A (or δ_l^B). $N_j^{s_A}$ (or $N_l^{q_B}$) represents the SD integer ambiguity. The ionospheric delay corresponding to the first frequency is represented by I^{s_A} (or I^{q_B}) and is linked to the observables by introducing a frequency-dependent coefficient of $\mu_j^A = (\lambda_j^A/\lambda_1^A)^2$ (or $\mu_l^B = (\lambda_l^B/\lambda_1^B)^2$).

Importantly, the receiver code and phase delays that remain after single differencing lead to rank defects in the observation equations. We can obtain full-rank equations by using *S*-system theory (Odolinski et al. 2014a; Odolinski and Teunissen 2016). The DD RTK model can be divided into classical differencing and inter-system differencing. In classical DD differencing, each system independently selects the reference satellite, whereas in DD inter-system differencing multiple systems share the same reference satellite (Deng et al. 2014). For the SD RTK model, no matter if classical differencing or the inter-system differencing, each system should select its own reference satellite in order to eliminate the rank deficiency between the phase delays and ambiguities. The difference between the classical differencing and the inter-system differencing in case of the SD model lies in the elimination of the other two kinds of rank deficiencies. Regarding the rank deficiencies caused by the linear dependency of the receiver clock and code/phase delays and that of the clocks, code/phase delays and ionosphere, it is common practice to eliminate them by selecting *S*-basis per constellation, leading to the model equivalent to the SD classical differencing. However, this approach does not fully exploit the advantages of using multi-GNSS signals. Alternatively, we can select unknown parameters pertaining to merely one constellation as the *S*-basis to eliminate the rank deficiencies; this approach can be characterized as SD

Table 1 Numbers of rank deficiencies and the *S*-basis choices for the ionospheric-float, ionospheric-fixed and ionospheric-weighted models of two GNSS constellations with classical and inter-system differencing

Model	Rank deficiencies	*S*-basis choice
Ionospheric-float with classical differencing	$4+f_A+f_B$	$d_1^A, d_2^A, N_j^{1_A}, d_1^B, d_2^B, N_l^{1_B}$
Ionospheric-float with inter-system differencing	$2+f_A+f_B$	$d_1^A, d_2^A, N_j^{1_A}, N_l^{1_B}$
Ionospheric-fixed/weighted with classical differencing	$2+f_A+f_B$	$d_1^A, N_j^{1_A}, d_1^B, N_l^{1_B}$
Ionospheric-fixed/weighted with inter-system differencing	$1+f_A+f_B$	$d_1^A, N_j^{1_A}, N_l^{1_B}$

Table 2 Estimable unknown parameters and their interpretations in the ionospheric-float model

Notation and interpretation	Estimable parameter
$\mathrm{d}\tilde{t} = \mathrm{d}t + \frac{\mu_2^A}{\mu_2^A-\mu_1^A} d_1^A - \frac{\mu_1^A}{\mu_2^A-\mu_1^A} d_2^A$	Relative receiver clock with the code bias of GNSS A, where $j=1, 2$
$\tilde{d}_j^A = d_j^A - \frac{\mu_2^A-\mu_j^A}{\mu_2^A-\mu_1^A} d_1^A + \frac{\mu_1^A-\mu_j^A}{\mu_2^A-\mu_1^A} d_2^A$	Relative receiver code bias of GNSS A, where $j \geq 3$
$\tilde{\delta}_j^A = \delta_j^A - \frac{\mu_2^A+\mu_j^A}{\mu_2^A-\mu_1^A} d_1^A + \frac{\mu_1^A+\mu_j^A}{\mu_2^A-\mu_1^A} d_2^A + \lambda_j^A N_j^{1_A}$	Relative receiver phase bias of GNSS A, where $j \geq 1$
$\tilde{d}_l^B = d_l^B - \frac{\mu_2^A-\mu_l^B}{\mu_2^A-\mu_1^A} d_1^A + \frac{\mu_1^A-\mu_l^B}{\mu_2^A-\mu_1^A} d_2^A$	Relative receiver code bias of GNSS B, where $l \geq 1$
$\tilde{\delta}_l^B = \delta_l^B - \frac{\mu_2^A+\mu_l^B}{\mu_2^A-\mu_1^A} d_1^A + \frac{\mu_1^A+\mu_l^B}{\mu_2^A-\mu_1^A} d_2^A + \lambda_l^B N_l^{1_B}$	Relative receiver phase bias of GNSS B, where $l \geq 1$
$\tilde{I}^{s_A} = I^{s_A} + \frac{d_2^A-d_1^A}{\mu_2^A-\mu_1^A}$ or $\tilde{I}^{q_B} = I^{q_B} + \frac{d_2^A-d_1^A}{\mu_2^A-\mu_1^A}$	Relative ionospheric delays biased by between-receiver differential code biases
$N_j^{1s_A} = N_j^{s_A} - N_j^{1_A}$ or $N_j^{1q_B} = N_l^{q_B} - N_l^{1_B}$	DD integer ambiguities, where $j \geq 1, l \geq 1, s \geq 2$ and $q \geq 2$

inter-system differencing. Both the classical differencing and the inter-system differencing in this paper are based on the SD model. The numbers of rank defects and the choices of the *S*-basis for the SD ionospheric-float, ionospheric-weighted and ionospheric-fixed models with both classical and inter-system differencing are given in Table 1. From the table, we see that the rank deficiencies in the case of inter-system differencing are less than in the classical differencing case.

After resolving the rank deficiencies, we obtain the inter-system differencing SD full-rank observation equations for the ionospheric-float model as follows:

$$\begin{aligned} E\left\{p_j^{s_A}\right\} &= g^{s_A}x_r + \mathrm{d}\tilde{t} + \tilde{d}_j^A + \mu_j^A \tilde{I}^{s_A} \\ E\left\{\phi_j^{s_A}\right\} &= g^{s_A}x_r + \mathrm{d}\tilde{t} + \tilde{\delta}_j^A + \lambda_j^A N_j^{1s_A} - \mu_j^A \tilde{I}^{s_A} \\ E\left\{p_l^{q_B}\right\} &= g^{q_B}x_r + \mathrm{d}\tilde{t} + \tilde{d}_l^B + \mu_l^B \tilde{I}^{q_B} \\ E\left\{\phi_l^{q_B}\right\} &= g^{q_B}x_r + \mathrm{d}\tilde{t} + \tilde{\delta}_l^B + \lambda_l^B N_l^{1q_B} - \mu_l^B \tilde{I}^{q_B} \end{aligned} \tag{2}$$

where the meaning of the reparametrized estimable unknowns is given in Table 2.

Since (2) now represents a full-rank system, the ionospheric-float code or phase ISB can be made available through differencing the SD code or phase observations between the two constellations, which can be expressed as

$$\begin{aligned} E\left\{\tilde{p}_{jl}^{s_A q_B}\right\} &= \tilde{d}_{jl}^{AB} + \mu_{jl}^{AB} I^{s_A q_B} \\ E\left\{\tilde{\phi}_{jl}^{s_A q_B}\right\} &= \tilde{\delta}_{jl}^{AB} + \lambda_{jl}^{AB} N_{jl}^{AB} - \mu_{jl}^{AB} I^{s_A q_B} \end{aligned} \tag{3}$$

where $\tilde{p}_{jl}^{s_A q_B} = p_l^{q_B} - p_j^{s_A} + (g^{s_A} - g^{q_B})x_r$, $\tilde{\phi}_{jl}^{s_A q_B} = \phi_l^{q_B} - \phi_j^{s_A} + (g^{s_A} - g^{q_B})x_r$, and the baseline is precisely determined using the whole observation series. In addition, $\tilde{d}_{jl}^{AB}$ and $\tilde{\delta}_{jl}^{AB}$

Table 3 Estimable unknown parameters and their interpretations for ISB estimation in the ionospheric-float model

Notation and interpretation	Estimable parameter
$\tilde{d}_{jl}^{AB} = d_{jl}^{AB} - \frac{\mu_2^A-\mu_l^B}{\mu_2^A-\mu_1^A} d_1^A + \frac{\mu_1^A-\mu_l^B}{\mu_2^A-\mu_1^A} d_2^A$	Estimable (but biased) code ISB of the ionospheric-float model
$\tilde{\delta}_{jl}^{AB} = \delta_{jl}^{AB} + \frac{\mu_1^B-\mu_j^A}{\mu_2^A-\mu_1^A}(d_2^A - d_1^A) + \lambda_{jl}^{AB} N_{jl}^{1_{AB}}$	Estimable (but biased) phase ISB of the ionospheric-float model
$\mu_{jl}^{AB} I^{s_A q_B} = \mu_l^B I^{q_B} - \mu_j^A I^{s_A}$	Ionospheric parameters
$\lambda_{jl}^{AB} N_{jl}^{AB} = \lambda_l^B N_l^{1q_B} - \lambda_j^A N_j^{1s_A}$	DD ambiguity parameters

are the estimable code and phase ISB, respectively, of the ionospheric-float model. The interpretations of the estimable unknowns in (3) are given in Table 3.

It is rather impractical to obtain epoch-by-epoch estimates of the ionospheric-float ISB because this model is too weak to guarantee successful integer ambiguity resolution. With this in mind, we present only the estimability of the ionospheric-float ISB but no further numerical analysis of their stability.

Estimation of ISB using the ionospheric-fixed model

Considering a baseline of zero or a short baseline of a few kilometers, one can safely assume canceling of ionospheric effects, thereby increasing the redundancy and strengthening the model (Odolinski and Teunissen 2017; Odolinski et al. 2014b). Once the rank deficiencies in Table 1 have been resolved, the ionospheric-fixed full-rank observation equations with inter-system differencing are given as follows:

$$\begin{aligned} E\left\{p_j^{s_A}\right\} &= g^{s_A}x_r + \mathrm{d}\tilde{\tilde{t}} + \tilde{\tilde{d}}_j^A \\ E\left\{\phi_j^{s_A}\right\} &= g^{s_A}x_r + \mathrm{d}\tilde{\tilde{t}} + \tilde{\tilde{\delta}}_j^A + \lambda_j^A N_j^{1_{s_A}} \\ E\left\{p_l^{q_B}\right\} &= g^{q_B}x_r + \mathrm{d}\tilde{\tilde{t}} + \tilde{\tilde{d}}_l^B \\ E\left\{\phi_l^{q_B}\right\} &= g^{q_B}x_r + \mathrm{d}\tilde{\tilde{t}} + \tilde{\tilde{\delta}}_l^B + \lambda_l^B N_l^{1_{q_B}} \end{aligned} \tag{4}$$

where the estimable unknowns are denoted by a double tilde. Similar to Table 2, Table 4 gives the descriptions of the unknown parameters and their meaning.

Many bias parameters can be estimated using (4), such as the between-receiver differential code biases and between-receiver differential phase biases of each GNSS (Liu et al. 2004; Zhang et al. 2016, 2017), but such estimation is not the focus of this research. Taking the differences of the code or phase observations between the two constellations yields the ISB. With (4), we can easily obtain the ISB estimation expressions for the ionospheric-fixed model, which read as follows:

$$\begin{aligned} E\left\{\tilde{p}_{jl}^{s_A q_B}\right\} &= \tilde{\tilde{d}}_{jl}^{AB} \\ E\left\{\tilde{\phi}_{jl}^{s_A q_B}\right\} &= \tilde{\tilde{\delta}}_{jl}^{AB} + \lambda_{jl}^{AB} N_{jl}^{AB} \end{aligned} \tag{5}$$

where $\tilde{\tilde{d}}_{jl}^{AB}$ and $\tilde{\tilde{\delta}}_{jl}^{AB} = \delta_{jl}^{AB} + \lambda_{jl}^{AB} N_{jl}^{1_{AB}}$ are the estimable code and phase ISB, respectively, of the ionospheric-fixed model. $\lambda_{jl}^{AB} N_{jl}^{AB} = \lambda_l^B N_l^B - \lambda_j^A N_j^A$ is, in essence, the geometry-free combination of two integer DD ambiguities. This fact motivates us to estimate the ISB in two steps.

Based on (4), the first step is to resolve the DD ambiguities $\lambda_l^B N_l^B$ and $\lambda_j^A N_j^A$, which can be precisely determined by using the whole observation series. For a zero or short baseline, we consider this task to be very easy. Once $\lambda_l^B N_l^B$ and $\lambda_j^A N_j^A$ have been resolved, $\lambda_{jl}^{AB} N_{jl}^{AB}$ can naturally be solved.

The second step is to substitute the DD ambiguities from $\tilde{\phi}_{jl}^{sq}$, which are precisely determined in the first step, thus yielding

$$\begin{aligned} E\left\{\bar{p}_{jl}^{s_A q_B}\right\} &= \tilde{\tilde{d}}_{jl}^{AB} \\ E\left\{\bar{\phi}_{jl}^{s_A q_B}\right\} &= \tilde{\tilde{\delta}}_{jl}^{AB} \end{aligned} \tag{6}$$

where $\bar{p}_{jl}^{s_A q_B} = \tilde{p}_{jl}^{s_A q_B}$ and $\bar{\phi}_{jl}^{s_A q_B} = \tilde{\phi}_{jl}^{s_A q_B} - \lambda_{jl}^{AB} N_{jl}^{AB}$. We conclude this step by solving for $\tilde{\tilde{d}}_{jl}^{AB}$ and $\tilde{\tilde{\delta}}_{jl}^{AB}$ using least-squares estimation.

Note that $\tilde{\tilde{\delta}}_{jl}^{AB} = \delta_{jl}^{AB} + \lambda_{jl}^{AB} N_{jl}^{1_{AB}}$, where the datum ambiguity $N_{jl}^{1_{AB}}$ corresponds to the reference satellite. When the observation period exceeds a few tens of hours, it will inevitably be necessary to assign multiple satellites as the reference, which may result in abrupt jumps in the phase ISB estimates. Considering this, we adopt a processing strategy without reference satellite changing. The SD ambiguity of the reference satellite is selected as the *S*-basis to resolve the rank deficiencies between the phase delays and ambiguities in the first epoch. Thus, when the reference satellite disappears, the remaining ambiguities still absorb the SD ambiguity of the reference satellite. Therefore, it is not necessary to add a new reference satellite to maintain the integer ambiguity property.

Table 4 Estimable unknown parameters and their interpretations in the ionospheric-fixed and ionospheric-weighted models

Notation and interpretation	Estimable parameter
$\mathrm{d}\tilde{\tilde{t}} = \mathrm{d}t + d_1^A$	Relative receiver clock with the code bias of GNSS A on $j = 1$
$\tilde{\tilde{d}}_j^A = d_j^A - d_1^A$	Relative receiver code bias of GNSS A, where $j \geq 2$
$\tilde{\tilde{\delta}}_j^A = \delta_j^A - d_1^A + \lambda_j^A N_j^{1_A}$	Relative receiver phase bias of GNSS A, where $j \geq 1$
$\tilde{\tilde{d}}_l^B = d_l^B - d_1^A$	Relative receiver code bias of GNSS B, where $l \geq 1$
$\tilde{\tilde{\delta}}_l^B = \delta_l^B - d_1^A + \lambda_l^B N_l^{1_B}$	Relative receiver phase bias of GNSS B, where $l \geq 1$
$N_j^{1_{s_A}} = N_j^{s_A} - N_j^{1_A}$ or $N_l^{1_{q_B}} = N_l^{q_B} - N_l^{1_B}$	DD integer ambiguities, where $j \geq 1, l \geq 1, s \geq 2$ and $q \geq 2$

Estimation of ISB using the ionospheric-weighted model

For this model, the S-basis choice is equivalent to that for the ionospheric-fixed model, so we can obtain the full-rank ionospheric-weighted model with inter-system differencing very quickly, as follows:

$$\begin{aligned} E\left\{p_j^{s_A}\right\} &= g^{s_A}x_r + \mathrm{d}\tilde{t} + \tilde{\tilde{d}}_j^A + \mu_j^A I^{s_A} \\ E\left\{\phi_j^{s_A}\right\} &= g^{s_A}x_r + \mathrm{d}\tilde{t} + \tilde{\tilde{\delta}}_j^A + \lambda_j^A N_j^{1s_A} - \mu_j^A I^{s_A} \\ E\left\{\bar{I}^{s_A}\right\} &= I^{s_A} \\ E\left\{p_l^{q_B}\right\} &= g^{q_B}x_r + \mathrm{d}\tilde{t} + \tilde{\tilde{d}}_l^B + \mu_l^B I^{q_B} \\ E\left\{\phi_l^{q_B}\right\} &= g^{q_B}x_r + \mathrm{d}\tilde{t} + \tilde{\tilde{\delta}}_l^B + \lambda_l^B N_l^{1q_B} - \mu_l^B I^{q_B} \\ E\left\{\bar{I}^{q_B}\right\} &= I^{q_B} \end{aligned} \tag{7}$$

where $\bar{I}^{s_A}$ (or $\bar{I}^{q_B}$) denotes additional ionospheric observables, which can be obtained through various methods, such as the Klobuchar model, the global ionospheric maps (GIM) model or a nearby reference network (Odijk 2014; Wang et al. 2016a; Wielgosz 2010). Since we mainly focus on a medium baseline of 10–60 km and there may be no reference network available nearby, we use a simple setup in which the observations of the ionosphere are set to zero so that we do not rely on any external ionospheric information. In addition, the SD ionospheric variance is modeled as a function of the baseline length as 0.96 mm/km (Odolinski et al. 2015; Mi et al. 2019).

Similar to the ISB estimation in the ionospheric-fixed model, we directly present the equations for ISB estimation in the ionospheric-weighted model as follows:

$$\begin{aligned} E\left\{\bar{p}_{jl}^{s_A q_B}\right\} &= \tilde{\tilde{d}}_{jl}^{AB} + \mu_{jl}^{AB} I^{s_A q_B} \\ E\left\{\bar{\phi}_{jl}^{s_A q_B}\right\} &= \tilde{\tilde{\delta}}_{jl}^{AB} - \mu_{jl}^{AB} I^{s_A q_B} \\ E\left\{\bar{I}^{s_A q_B}\right\} &= I^{s_A q_B} \end{aligned} \tag{8}$$

where the meaning of the ISB is the same as those in the ionospheric-fixed model. For ISB estimation using the ionospheric-weighted model, the same two-step method used with the ionospheric-fixed model is again adopted.

Experimental results

In this section, we will analyze the stability of the ISB from GPS/BDS/Galileo data for several pairs of multi-GNSS receivers of various types. To achieve our goal, two experiments were carried out. The first one was a zero/short-baseline experiment based on the ionospheric-fixed model, and the second was a medium-baseline experiment based on the ionospheric-weighted model. Afterward, experiments were conducted to analyze the effects of the ISB on RTK positioning.

Unless otherwise specified, the sampling interval of the experimental GNSS observations was 30 s, and the cutoff elevation mask was 15°. These observations were weighted in accordance with a stochastic model calculated using variance component estimation (VCE) (Teunissen and Amiri-Simkooei 2007; Tiberius and Kenselaar 2013).

Zero/short-baseline experiment

For our analysis, we selected GNSS data from several receivers. Each set of received multi-constellation data was measured over three consecutive days. Table 5 summarizes the relevant characteristics of the experimental data sets that were considered in our analysis, including the station name, the receiver and antenna types, the approximate locations of the receivers and the time period of the observations. Two baselines were formed with three receivers: CUT0–CUT2 (with the same receiver type) and CUT0–CUT3 (with different receiver type).

In this section, the code and phase ISB are estimated for several different frequency combinations, including the L1–E1 and L2–E5a of GPS and Galileo as well as the L1–B1 and L2–B2 of GPS and BDS. Note that only the GPS L1 and Galileo E1 bands have overlapping frequencies, whereas the other ISB estimates are based on non-overlapping frequencies.

Figures 1 and 2 show the estimated GPS–Galileo ISB for CUT0–CUT2 and CUT0–CUT3 for three days (DOY 324, 325 and 326 of 2018). By focusing on each panel, these estimates fluctuate randomly around their mean values with no apparent trend over time. We first focus on the case depicted in Fig. 1 (with the same receiver type), from which two conclusions can be drawn. First, regardless of whether

Table 5 Overview of the GNSS data used in the zero/short-baseline experiment

Station name	Receiver type	Antenna type	Location	Observation period
CUT0	TRIMBLE NETR9	TRM59800.00	115.89°E, 32.00°S	2018, days 324–326
CUT0	TRIMBLE NETR9	TRM59800.00	115.89°E, 32.00°S	2018, days 324–326
CUT2	TRIMBLE NETR9			
CUT3	Javad TRE_G3TH_8			

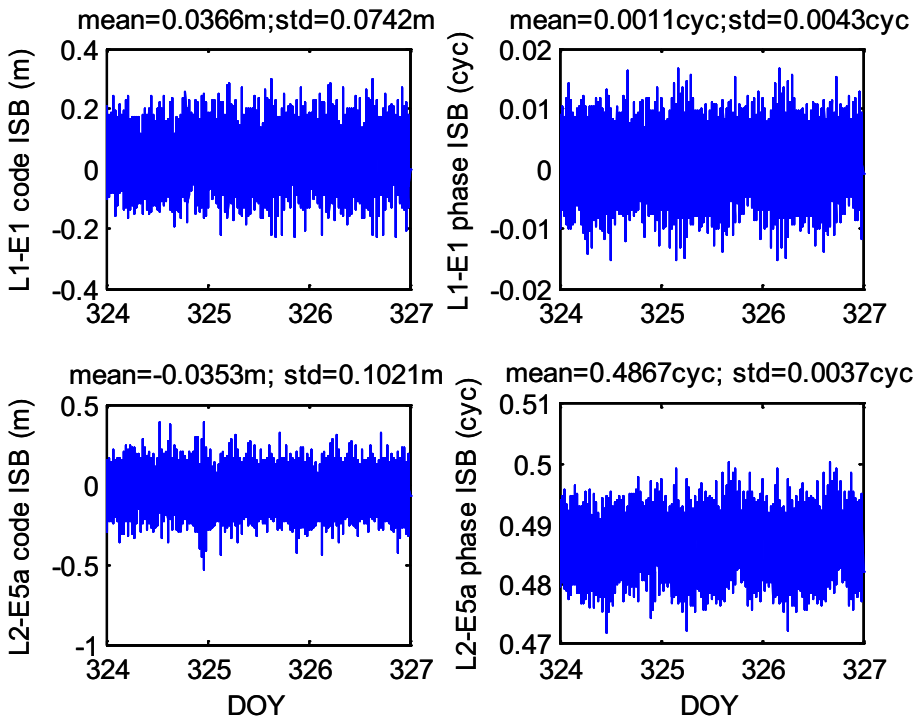

Fig. 1 Estimated differential ISB for L1–E1 (top) and L2–E5a (bottom) for CUT0–CUT2

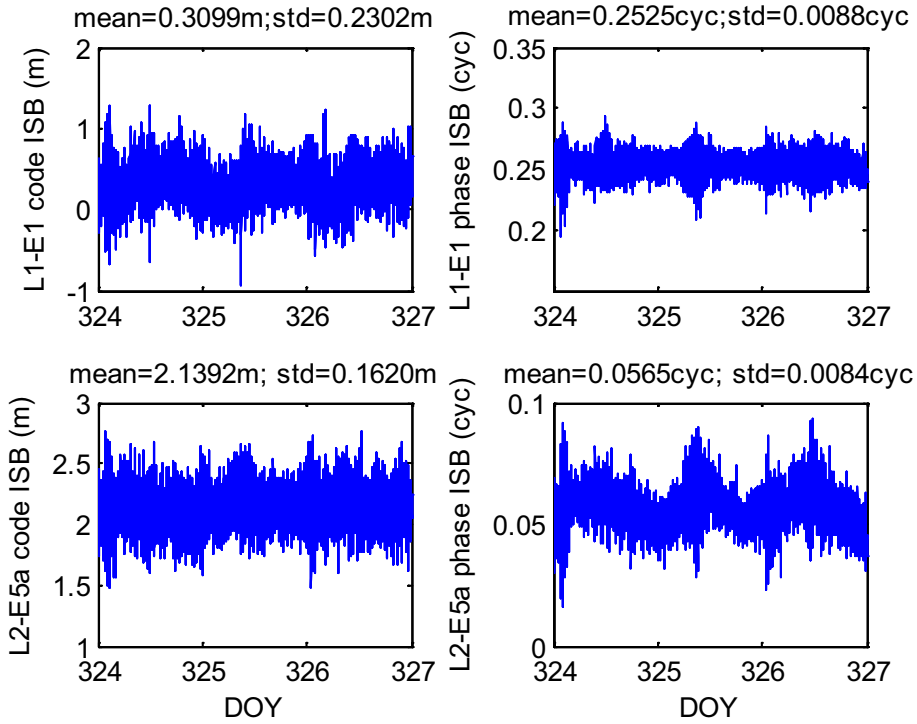

Fig. 2 Estimated differential ISB for L1–E1 (top) and L2–E5a (bottom) for CUT0–CUT3

there are overlapping frequencies, the code ISB for receivers of the same type can be safely considered to be within the noise of the observations. Second, the phase ISB are different from the code ISB, showing different results for the cases of overlapping and non-overlapping frequencies. The phase ISB for the overlapping frequency case has a mean of practically zero, while the mean phase ISB in the non-overlapping frequency case is completely different. Figure 2 depicts the remaining cases (with different receiver types), based on which our findings can be extended as follows. The

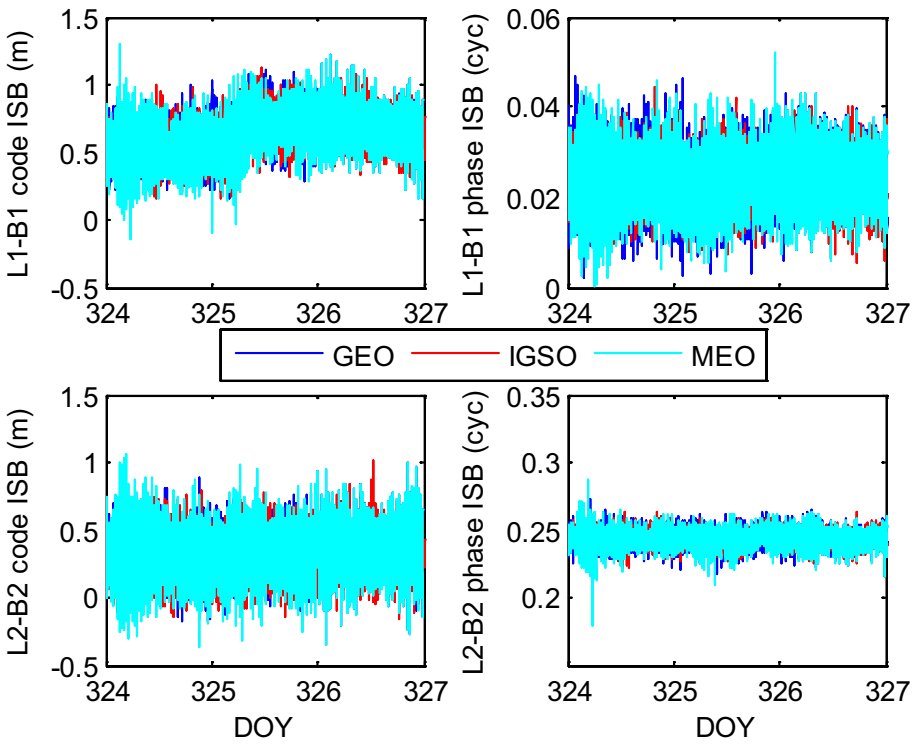

Fig. 3 Estimated differential ISB for L1–B1 (top) and L2–B2 (bottom) for CUT0–CUT2 in the GEO, IGSO and MEO cases

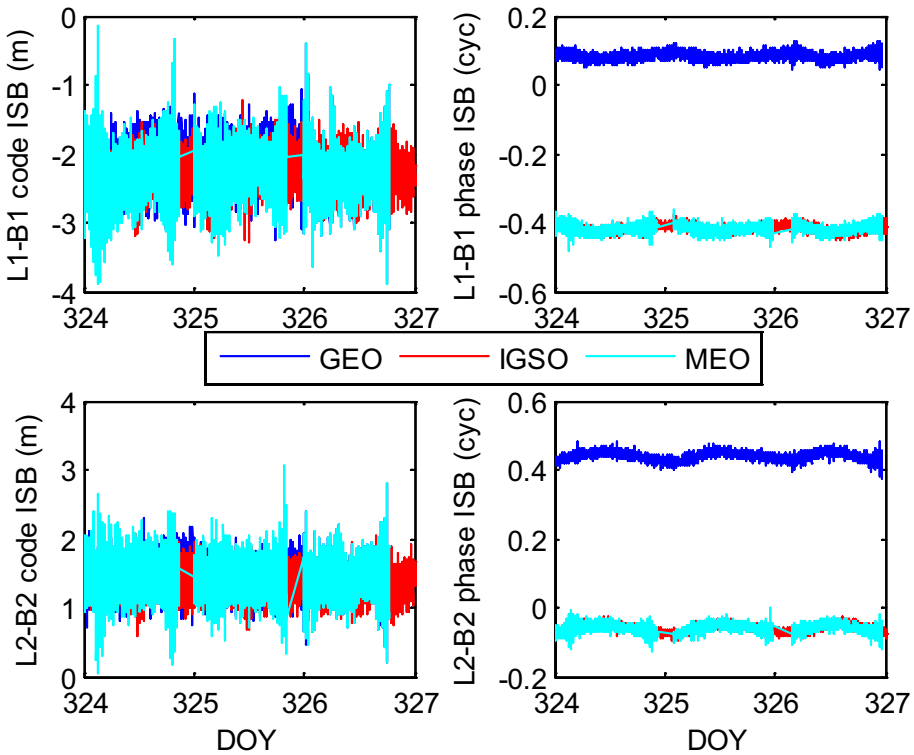

Fig. 4 Estimated differential ISB for L1–B1 (top) and L2–B2 (bottom) for CUT0–CUT3 in the GEO, IGSO and MEO cases

values of the code and phase ISB are significant regardless of whether there are overlapping frequencies; thus, we are forced to consider their impacts in a mixed model.

Figures 3 and 4 show the 3-day time series of the estimated GPS–BDS ISB for CUT0–CUT2 and CUT0–CUT3, where the differences between MEO, GEO and IGSO are considered for BDS. Note that there is no overlap between

Table 6 Statistics of the estimated L1–B1 and L2–B2 ISB for GEO, IGSO and MEO

Baseline	Frequency	Code ISB (m)		Phase ISB (cycle)	
		Mean	SD	Mean	SD
CUT0	L1–B1	0.633	0.144	0.024	0.005
CUT2	L2–B2	0.331	0.149	0.243	0.005
	L1–B1	− 2.214 (GEO)	0.304 (GEO)	0.083 (GEO)	0.010 (GEO)
		− 2.272 (IGSO)	0.243 (IGSO)	− 0.417 (IGSO and MEO)	0.012 (IGSO and MEO)
CUT0		− 2.307 (MEO)	0.343 (MEO)		
CUT3	L2–B2	1.425 (GEO)	0.221 (GEO)	0.440 (GEO)	0.011 (GEO)
		1.365 (IGSO)	0.183 (IGSO)	− 0.060 (IGSO and MEO)	0.012 (IGSO and MEO)
		1.445 (MEO)	0.270 (MEO)		

the GPS and BDS-2 frequencies; thus, we expect this to be similar to the L2–E5a in the GPS–Galileo case. As shown in Fig. 3, both the code and phase ISB are stable, and their values are significant. In addition, we note that the GEO, IGSO and MEO results show good consistency, which means that there is no reason to expect inter-system satellite biases (ISTB) to be present for baselines between receivers of the same type; hence, they can be ignored in a mixed model. However, the case is different for baselines between receivers of different types. In Fig. 4, we can intuitively see that the GEO, IGSO and MEO results are different in terms of the phase ISB. Note that the correlation between the time series of the GPS–IGSO phase ISB estimates and that of the GPS–MEO estimates is quite striking, suggesting that there is no phase ISTB between IGSO and MEO. We further support this finding by providing the corresponding statistics in Table 6. However, as seen from the statistics in this table, there is a 0.5-cycle difference between the GPS–GEO and GPS–IGSO/MEO phase ISB. Given this fact, it is natural to suspect that there is a half-cycle phase ISTB between GEO and IGSO/MEO.

Medium-baseline experiment

The medium-baseline experiment was conducted based on data collected and provided by the Hong Kong Satellite Positioning Reference Station Network (SatRef), as detailed in Table 7. Here, we analyzed only the feasibility of ISB estimation using the ionospheric-weighted model with a medium baseline. For convenience and simplicity, we present the results from only a portion of the test stations over a selected window of time during our test period (DOY 316 of 2018). These results are representative of all the experimental results that we obtained.

In previous investigations, the ISB between overlapping frequencies of receivers from different manufacturers (Trimble, Lecia, Javad and Septentrio) were analyzed based on zero/short baselines, and the conclusion was drawn that the ISB are stable on a time scale of days (Odijk and Teunissen 2013). Now that we know the stability of the ISB, we can adjust our estimation strategy by using Kalman filter.

Figure 5 and Table 8 show the time series and statistics of the GPS–Galileo ISB for each of the four baselines. With this information, we can extend our findings while validating our previous findings. First, the most important point to note is that ISB can be feasibly estimated using a medium baseline, as seen from the fact that according to the statistics in the table, the estimated ISB fall safely within the noise of the observations. Second, for the HKTK–HKQT and HKTK–HKKT baselines, which are between receivers of the same type and different types, respectively, the findings are consistent with the findings for the previous short-baseline condition.

Attention should be focused on the HKKS–HKKT and HKKT–HKSL baselines, for which both receivers are of the Leica GR50 type; we therefore expect similar results to those found previously, but in fact, they are completely different. Figure 5 shows that the results for these two baselines are not very consistent for the L2–E5a (for both the code and phase ISB), as verified by the statistics in the table. The reason for this finding is that although the receiver type of HKKS

Table 7 Baselines and the corresponding receiver types in the medium-baseline experiment

Baseline	Receiver 1	Receiver 2	Base length/km
HKTK–HKKT	Trimble NetR9	Leica GR50 (4.30/7.402)	19.7
HKKS–HKKT	Leica GR50 (4.20/7.300)	Leica GR50 (4.30/7.402)	26.7
HKKT–HKSL	Leica GR50 (4.30/7.402)	Leica GR50 (4.30/7.402)	16.4
HKTK–HKQT	Trimble NetR9	Trimble NetR9	28.3

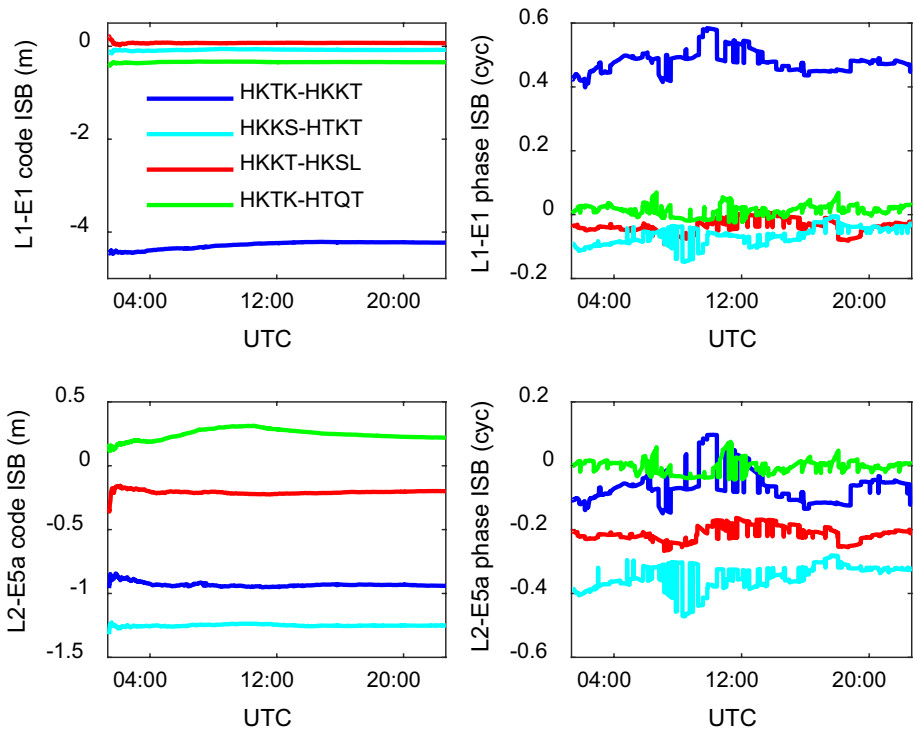

Fig. 5 Estimated differential ISB for L1–E1 (top) and L2–E5a (bottom) for four baselines on DOY 316 of 2018

Table 8 Statistics of the L1–E1 and L2–E5a ISB estimated using the ionospheric-weighted model for HKTK–HKKT, HKKS–HKKT, HKKT–HKSL and HKTK–HKQT

Baseline	Frequency	Code ISB (m)		Phase ISB (cyc)	
		Mean	SD	Mean	SD
HKTK–HKKT	L1–E1	−4.279	0.075	0.480	0.036
	L2–E5a	−0.931	0.017	−0.064	0.054
HKKS–HKKT	L1–E1	−0.017	0.011	−0.066	0.029
	L2–E5a	−1.250	0.007	−0.348	0.038
HKKT–HKSL	L1–E1	−0.012	0.011	−0.036	0.023
	L2–E5a	−0.207	0.014	−0.212	0.022
HKTK–HKQT	L1–E1	−0.341	0.009	0.014	0.017
	L2–E5a	0.246	0.040	−0.002	0.022

was the same as that of the other two receivers (HKKT and HKSL), the firmware version was different, leading to different results. To verify this, we conducted several additional experiments, which also supported the conclusion that the ISB depend on the firmware version.

Impact of ISB on RTK positioning

It should be emphasized again that the purpose of ISB calibration is to analyze the stability of the ISB and, more importantly, to improve the positioning performance. To be more specific, we need to consider the ISB when performing RTK positioning for mixed constellations to improve the ambiguity resolution performance. For this purpose, three baselines were tested, namely CUT0–CUAI, HKQT–HKKT and HKTK–HKNP, corresponding to short, medium and long baselines, respectively. The details of the three baselines are given in Table 9.

We carried out experiments with both classical and inter-system differencing. For each method, we tested two different signal combination modes, namely GPS + Galileo and GPS + Galileo + BDS. In these experiments, the ISB were treated as time-invariant parameters because of their stability. However, even under such conditions, it is difficult to achieve fast ambiguity fixing for long baselines; therefore, we also consider another indicator, namely the time to first fix (TTFF).

Table 9 Overview of the GNSS data for the three baselines used in the positioning experiments

Baseline	Constellation and frequency	Length/km	Location	Observation period
CUT0–CUAI (Trimble–Javad)	GPS L1, L2 BDS B1, B2 Galileo E1, E5a	0.008	Perth, Australia	DOY 318, 2018
HKQT–HKTK (Trimble–Leica)		28.3	Hong Kong, China	DOY 328, 2018
HKTK–HKNP (Trimble–Leica)		47.3	Hong Kong, China	DOY 328, 2018

Table 10 Empirical integer ambiguity success rates for the short baseline CUT0–CUAI

System	Classical differencing	Inter-system differencing
GPS + Galileo	1808/2880 = 62.8%	2546/2880 = 88.4%
GPS + Galileo + BDS	2061/2880 = 71.6%	2834/2880 = 98.4%

Since the CUT0–CUAI baseline is short and the instantaneous ambiguity resolution is successful over the whole time period, the superiority of inter-system differencing cannot be seen with conventional data processing. Therefore, we set a cutoff elevation of 40° to simulate RTK in a complex environment. Table 10 presents the ambiguity resolution statistics in terms of empirical success rates. The empirical success rate can be defined as,

$$P_{\mathrm{SE}} = \frac{\#\text{ of correctly fixed epochs}}{\text{total }\#\text{ of epochs}} \tag{9}$$

From Table 10, it can be seen that the availability of positioning solutions markedly increases in the case of inter-system differencing compared with classical differencing.

Figure 6 describes the positioning results obtained via classical differencing and inter-system differencing,

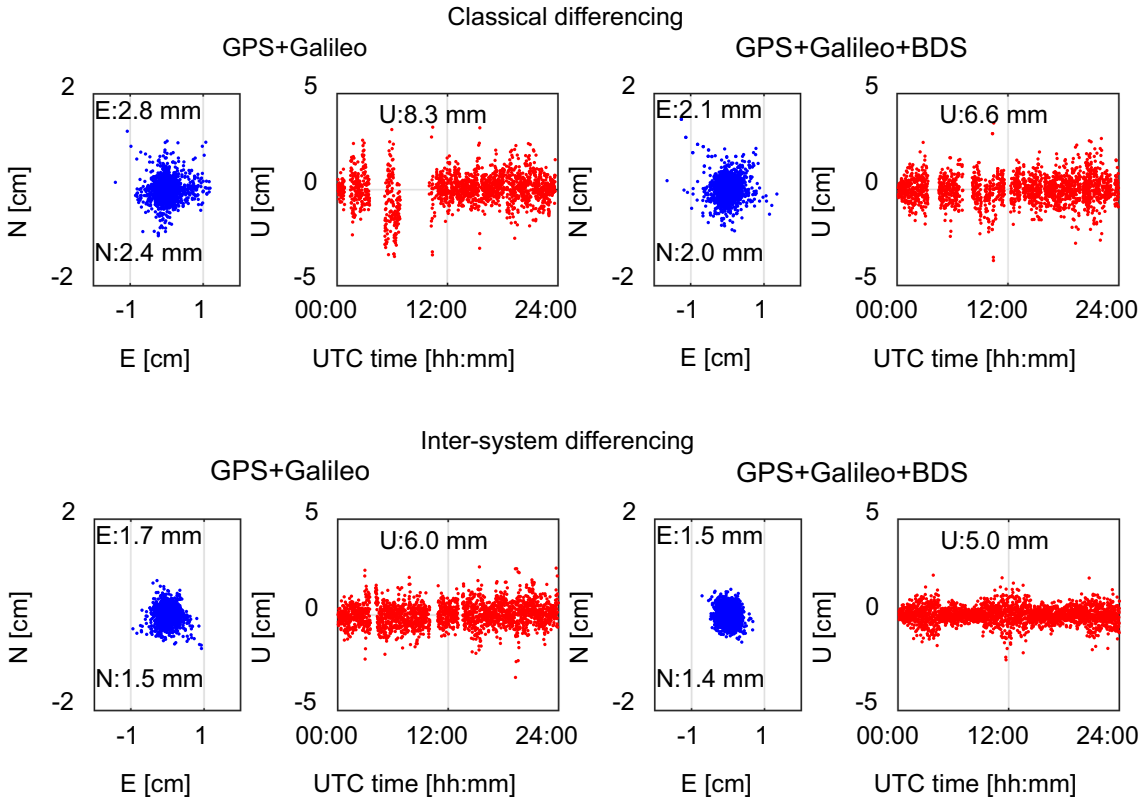

Fig. 6 Positioning results for CUT0–CUAI with classical differencing and inter-system differencing based on GPS + Galileo (top) and GPS + Galileo + BDS (bottom). Both horizontal position scatter and vertical time series are given

Table 11 Statistics of the positioning results for CUT0–CUAI using the ionospheric-fixed model, demonstrating the improvement achieved with inter-system differencing compared with classical differencing

System	RMS of the positioning errors (mm)						Improvement (%)		
	Classical differencing			Inter-system differencing					
	N	E	U	N	E	U	N	E	U
GE	2.4	2.8	8.3	1.5	1.7	6.0	37.5	39.3	27.7
GEC	2.0	2.1	6.6	1.4	1.5	5.0	30.0	28.6	24.2

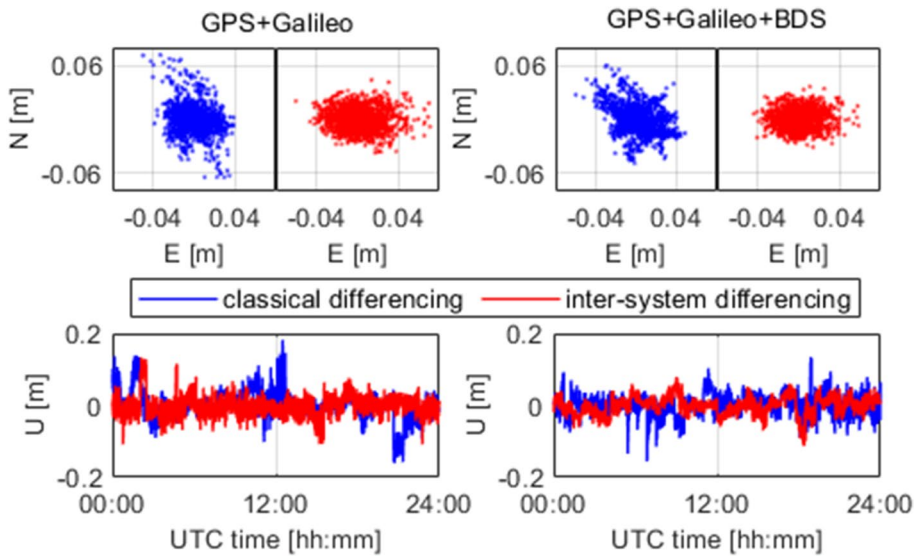

Fig. 7 Positioning results for HKQT–HKTK with classical differencing (blue) and inter-system differencing (red) based on GPS + Galileo (left) and GPS + Galileo + BDS (right) (color figure online)

Table 12 Statistics of the positioning results for HKQT–HKTK using the ionospheric-weighted model, demonstrating the improvement achieved with inter-system differencing compared with classical differencing

System	RMS of the positioning errors (mm)						Improvement (%)		
	Classical differencing			Inter-system differencing					
	N	E	U	N	E	U	N	E	U
GE	17.2	19.0	43.8	13.4	14.2	32.2	22.1	25.3	26.5
GEC	15.8	14.4	36.8	11.1	11.7	29.0	29.7	18.8	21.2

respectively, for CUT0–CUAI using the GPS + Galileo and GPS + Galileo + BDS combinations. The positioning errors were obtained by comparing the positioning results with the known coordinates. According to these graphs, the positioning result obtained via inter-system differencing is better than that obtained via classical differencing; this finding suggests that inter-system differencing can strengthen the position model. Table 11 presents the root mean square (RMS) statistics of the positioning errors for the CUT0–CUAI baseline, from which we can see that the positioning accuracy of the inter-system differencing is improved by approximately 30% compared with that of the classical differencing.

We performed an analysis similar to the short-baseline analysis on the medium-baseline HKQT–HKTK. Specifically, we used the ionospheric-weighted model and a cutoff elevation of 15°. Figure 7 and Table 12 present the positioning results obtained via classical differencing and inter-system differencing for the medium-baseline HKQT–HKTK. On the whole, the positioning results obtained via inter-system differencing are more stable than those obtained via classical differencing. For GPS + Galileo, the RMS values of the positioning errors of the classical differencing in the North/East/Up are 17.2, 19.0 and 43.8 mm, respectively, while the corresponding errors of the inter-system differencing are 13.4, 14.2 and 32.2 mm, representing improvements in 22.1, 25.3 and 26.5%, respectively. Similar conclusions can be drawn from the results for GPS + Galileo + BDS; hence, those results are not presented here.

Unlike in the short- and medium-baseline cases, it is difficult to achieve rapid ambiguity fixing in the case of a long baseline, but we believe that inter-system differencing still offers some improvement compared with classical differencing. The measure of merit that is considered is the TTFF, which is the time required before the first fixed solution can be accessed. Table 13 shows that, as expected, the

Table 13 TTFFs of the classical differencing and the inter-system differencing for HKTK–HKNP for both GPS + Galileo and GPS + Galileo + BDS

System	Number of epochs required (TTFF)		Improvement (%)
	Classical differencing	Inter-system differencing	
GPS + Galileo	29	22	24.1
GPS + Galileo + BDS	24	18	25.0

inter-system differencing takes some time to converge, but it is much faster (by approximately 25%) than the classical differencing.

Conclusions

In this study, we presented an inter-system biases (ISB) estimation method based on single-differenced (SD) observables and used *S*-system theory to construct full-rank functional models. The main contributions of this work include ISB estimation for non-overlapping frequencies and for medium baselines using the ionospheric-weighted model. Specifically, we analyzed the ISB stability of the GPS–Galileo and GPS–BDS, and the application of ISB in real-time kinematic (RTK) positioning.

In contrast to the double-differenced (DD) method, the proposed SD method can solve the problem of ISB estimation for non-overlapping frequencies. This fact is true, because the SD method differs from the DD method, in that the former selects the reference satellite per constellation, thereby giving rise to constellation-specific DD ambiguities. This difference leads to the important practical consequence that with our proposed methodology, one can estimate the ISB between any two frequencies without worrying about whether they overlap.

The ISB stability of the ionospheric-fixed and ionospheric-weighted models was analyzed by applying the SD method for both short and medium baselines, and the results suggest that the ISB remain stable throughout the day and can safely be considered to fall within the noise of the observations. We emphasize that the purpose of our work is not to estimate the ISB themselves but rather to improve the positioning precision of mixed constellations. Using the ISB as prediction parameters in RTK positioning can help to avoid catastrophic failure of ambiguity resolution, and the results suggest that the positioning accuracy can be improved by 20–35% compared with the accuracy achieved through classical differencing.

At present, the construction of global navigation satellite system (GNSS) has undergone dramatic changes, and we can foresee that the coming years will witness a proliferation of GNSS constellations and signals. Modeling or calibrating the ISB of different GNSS constellations to enhance their compatibility and interoperability will be a focus of our future work and will be essential for enabling high-precision mixed constellation RTK positioning.

Acknowledgments Many thanks are due to Curtin University and Hong Kong SatRef for providing GNSS data. This work was funded by the National Natural Science Foundation of China (Nos. 41604031, 41774042, and 41621091) and the National Key Research Program of China Collaborative Precision Positioning Project (No. 2016YFB0501900). The second author is supported by the CAS Pioneer Hundred Talents Program. The third author acknowledges the LU JIAXI International team program supported by the K.C. Wong Education Foundation and CAS.

References

Dalla Torre A, Caporali A (2015) An analysis of intersystem biases for multi-GNSS positioning. GPS Solut 19(2):297–307

Deng C, Tang W, Liu J, Shi C (2014) Reliable single-epoch ambiguity resolution for short baselines using combined GPS/BeiDou system. GPS Solut 18(3):375–386

Gao W, Gao C, Pan S, Meng X, Xia Y (2017) Inter-system differencing between GPS and BDS for medium-baseline RTK positioning. Remote Sens. https://doi.org/10.3390/rs9090948

Gioia C, Borio D (2016) A statistical characterization of the Galileo-to-GPS inter-system bias. J Geodesy 90(11):1279–1291

Jiang N, Xu Y, Xu T, Xu G, Sun Z, Schuh H (2017) GPS/BDS short-term ISB modelling and prediction. GPS Solut 21(1):163–175

Li X, Ge M, Dai X, Ren X, Fritsche M, Wickert J, Schuh H (2015) Accuracy and reliability of multi-GNSS real-time precise positioning: GPS, GLONASS, BeiDou, and Galileo. J Geodesy 89(6):607–635. https://doi.org/10.1007/s00190-015-0802-8

Li X, Li X, Yuan Y, Zhang K, Zhang X, Wickert J (2017) Multi-GNSS phase delay estimation and PPP ambiguity resolution: GPS, BDS, GLONASS, Galileo. J Geodesy 92(6):579–608. https://doi.org/10.1007/s00190-017-1081-3

Liu X, Tiberius C, de Jong K (2004) Modelling of differential single difference receiver clock bias for precise positioning. GPS Solut 7(4):209–221. https://doi.org/10.1007/s10291-003-0079-x

Liu T, Zhang B, Yuan Y, Li Z, Wang N (2018) Multi-GNSS triple-frequency differential code bias (DCB) determination with precise point positioning (PPP). J Geodesy. https://doi.org/10.1007/s00190-018-1194-3

Mi X, Zhang B, Yuan Y (2019) Stochastic modeling of between-receiver single-differenced ionospheric delays and its application to medium baseline RTK positioning. Meas Sci Technol. https://doi.org/10.1088/1361-6501/ab11b5

Nadarajah N, Teunissen PJG, Raziq N (2013) BeiDou inter-satellite-type bias evaluation and calibration for mixed receiver attitude determination. Sensors (Basel) 13(7):9435–9463. https://doi.org/10.3390/s130709435

Nadarajah N, Teunissen PJG, Sleewaegen J-M, Montenbruck O (2014) The mixed-receiver BeiDou inter-satellite-type bias and its impact on RTK positioning. GPS Solut 19(3):357–368. https://doi.org/10.1007/s10291-014-0392-6

Odijk D (2014) Improving ambiguity resolution by applying ionosphere corrections from a permanent GPS array. Earth Planets Space 52(10):675–680. https://doi.org/10.1186/bf03352262

Odijk D, Teunissen PJG (2012) Characterization of between-receiver GPS–Galileo inter-system biases and their effect on mixed ambiguity resolution. GPS Solut 17(4):521–533. https://doi.org/10.1007/s10291-012-0298-0

Odijk D, Teunissen PJG (2013) Estimation of differential inter-system biases between the overlapping frequencies of GPS, Galileo, BeiDou and QZSS. In: Proceedings of the 4th international colloquium scientific and fundamental aspects of the Galileo programme, Prague, Czech Republic, 4–6 Dec, p 8

Odijk D, Nadarajah N, Zaminpardaz S, Teunissen PJG (2016) GPS, Galileo, QZSS and IRNSS differential ISBs: estimation and application. GPS Solut 21(2):439–450. https://doi.org/10.1007/s10291-016-0536-y

Odolinski R, Teunissen PJG (2016) Single-frequency, dual-GNSS versus dual-frequency, single-GNSS: a low-cost and high-grade receivers GPS–BDS RTK analysis. J Geodesy 90(11):1255–1278. https://doi.org/10.1007/s00190-016-0921-x

Odolinski R, Teunissen PJG (2017) Low-cost, 4-system, precise GNSS positioning: a GPS, technology. https://doi.org/10.1088/1361-6501/aa92eb

Odolinski R, Teunissen PJG, Odijk D (2014a) Combined BDS, Galileo, QZSS and GPS single-frequency RTK. GPS Solut 19(1):151–163. https://doi.org/10.1007/s10291-014-0376-6

Odolinski R, Teunissen PJG, Odijk D (2014b) First combined COMPASS/BeiDou-2 and GPS positioning results in Australia. Part II: single- and multiple-frequency single-baseline RTK positioning. J Spat Sci 59(1):25–46. https://doi.org/10.1080/14498596.2013.866913

Odolinski R, Teunissen PJG, Odijk D (2015) Combined GPS + BDS for short to long baseline RTK positioning. Meas Sci Technol. https://doi.org/10.1088/0957-0233/26/4/045801

Paziewski J, Wielgosz P (2014) Accounting for Galileo–GPS inter-system biases in precise satellite positioning. J Geodesy 89(1):81–93. https://doi.org/10.1007/s00190-014-0763-3

Paziewski J, Sieradzki R, Wielgosz P (2015) Selected properties of GPS and Galileo–IOV receiver intersystem biases in multi-GNSS data processing. Meas Sci Technol 26(9):095008. https://doi.org/10.1088/0957-0233/26/9/09500

Teunissen PJG, Amiri-Simkooei AR (2007) Least-squares variance component estimation. J Geodesy 82(2):65–82. https://doi.org/10.1007/s00190-007-0157-x

Tian Y, Ge M, Neitzel F, Zhu J (2017) Particle filter-based estimation of inter-system phase bias for real-time integer ambiguity resolution. GPS Solut 21(3):949–961

Tiberius CCJM, Kenselaar F (2013) Estimation of the stochastic model for GPS code and phase observables. Surv Rev 35(277):441–454. https://doi.org/10.1179/sre.2000.35.277.441

Wang L, Feng Y, Guo J (2016a) Reliability control of single-epoch RTK ambiguity resolution. GPS Solut 21:591–604. https://doi.org/10.1007/s10291-016-0550-0

Wang N, Yuan Y, Li Z, Montenbruck O, Tan BF (2016b) Determination of differential code biases with multi-GNSS observations. J Geodesy 90(3):209–228

Wielgosz P (2010) Quality assessment of GPS rapid static positioning with weighted ionospheric parameters in generalized least squares. GPS Solut 15(2):89–99. https://doi.org/10.1007/s10291-010-0168-6

Zhang B, Teunissen PJG, Yuan Y (2016) On the short-term temporal variations of GNSS receiver differential phase biases. J Geodesy 91(5):563–572. https://doi.org/10.1007/s00190-016-0983-9

Zhang B, Liu T, Yuan Y (2017) GPS receiver phase biases estimable in PPP-RTK networks: dynamic characterization and impact analysis. J Geodesy 92(6):659–674. https://doi.org/10.1007/s00190-017-1085-z

Zhang B, Chen Y, Yuan Y (2018) PPP-RTK based on undifferenced and uncombined observations: theoretical and practical aspects. J Geodesy. https://doi.org/10.1007/s00190-018-1220-5

Xiaolong Mi is an M.Sc. student at the Institute of Geodesy and Geophysics at the Chinese Academy of Sciences. His current research interests include various biases involved in GNSS estimations and the weighting of the ionospheric-weighted model.

Baocheng Zhang is a research fellow at the Institute of Geodesy and Geophysics at the Chinese Academy of Sciences in Wuhan. His research focuses on multi-GNSS integer ambiguity resolution-enabled precise point positioning (PPP-RTK) with an emphasis on code and carrier phase bias estimation and characterization, ionospheric delay retrieval and prototype PPP-RTK network software development.

Yunbin Yuan is a professor and the director of the GNSS Application and Research Group at the Institute of Geodesy and Geophysics at the Chinese Academy of Sciences. His current research interests are the following: (1) GNSS-based spatial environmental monitoring and analysis, (2) high-precision GNSS satellite navigation and positioning and (3) GNSS applications to orbit determination for LEO satellites.